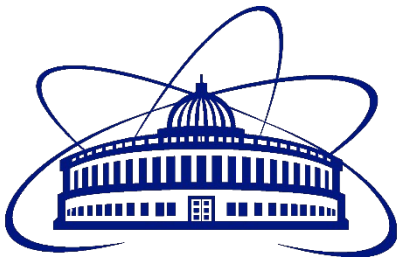

JOINT INSTITUTE FOR NUCLEAR RESEARCH
Veksler and Baldin laboratory of High Energy Physics

FINAL REPORT ON THE START PROGRAMME

Alignment of TOF-400 detector at BM@N experiment

Supervisor:
Mikhail Rumyantsev

Student:
Irina Zhavoronkova, student
National Research Nuclear University MEPhI

Participation period:
July 10 – August 27,
Summer Session 2023

Dubna, 2023

Содержание

Introduction

The BM@N (Baryonic Matter at the Nuclotron) is the first experiment at the accelerator complex of NICA-Nuclotron . Its main purpose is to investigate properties of nuclear matter under extreme density and temperature [1]. The Nuclotron provides the experiment with beams from protons up to Au ions, with a kinetic energy in the range from 1 to 6 GeV per nucleon. The maximum beam kinetic energy for ions with the charge to atomic weight ratio of 1/2 is 6 GeV per nucleon. The maximum kinetic energy of Au ions with Z/A ratio equals to 0.4 is 4.5 GeV per nucleon, while the maximum kinetic energy for protons is 13 GeV.

The BM@N is designed as a spectrometer capable of detecting charged hadrons, electrons and photons in heavy-ion collisions in the energy range of the Nuclotron. To reach this goal, the detector includes a precise tracking system and a high-performance particle identification system based on time-of-flight measurements and calorimetry.

The research program of the BM@N experiment is aimed to study heavy ion collisions at the Nuclotron including the following directions: investigation of the reaction dynamics and the equation of state of nuclear matter, production of strange and multi-strange hyperons close to the threshold and search for hyper-nuclei.

BM@N Experiment Setup

1. General description

A scheme of the BM@N experimental setup is shown in Figure 1. The experiment combines high precision track measurements with time-of-flight information for particle identification and calorimetry for the analysis of the collisions centrality. The magnetic field of the analyzing magnet can be varied up to 1 T to get the optimal detector acceptance and momentum resolution for different reactions and beam energies. The charged particle momentum and multiplicity are measured with the set of Gas Electron Multipliers (GEM) located inside the analyzing magnet. Double-sided Silicon tracking system (STS) is installed between the GEM tracker and the target to improve the track and vertex reconstruction in heavy ion collisions. STS and GEM together constitute the inner tracker system. The outer tracking system consists of six planes of cathode strip chambers (CSC). They are located outside the magnetic field and refine the track parameters, obtained using the GEM detectors. Besides the improvement of the particle momentum resolution, the CSC+GEM-based track is used to find corresponding hits in the ToF-400 and ToF-700 time-of-flight systems.

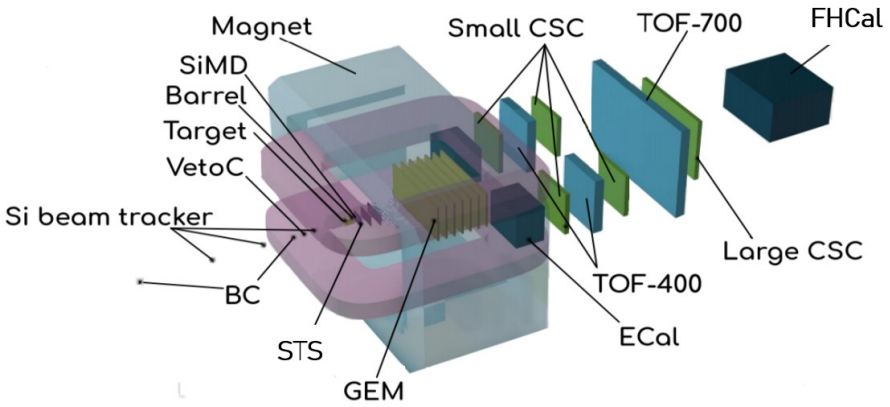

Fig. 1. Schematic view of the BM@N experimental setup: FwdSi – Forward double-sided silicon strip-detectors, STS – Silicon Tracking System; GEM – Gas Electron Multipliers, CSC – Cathode Strip Chambers, ToF-400, ToF-700 – Multi-gap Resistive Plate Chambers, ECAL – Electromagnetic Calorimeter, ZDC – Zero Degree Calorimeter.

FHCal is designed to determine the centrality of the collision and the orientation of the reaction plane for the study of collective flows [2]. FHCal consists of modules of two different sizes, with inner being smaller to improve energy resolution. The modules consist of lead/scintillator layers, and total length of modules corresponds to about 4 nuclear interaction lengths. To increase the accuracy of the centrality and angle of the reaction plane measurements, an additional detector in the FHCal beam hole is proposed, which is Cherenkov quartz hodoscope.

2. STS+GEM tracking system

The detector which is of our interest in the current work is TOF-400. However, the TOF-400 detector performance heavily relies on the inner tracking system performance. For this reason, more detailed description of the latter system is presented.

In the experiment the target is placed at $z=0$, and z axis has orientation such that the beam always goes along that z axis. Thus the interaction of the beam and the target occurs at $z=0$, and produced particle travel in forward direction along $z$axis.

The task of the hybrid STS-GEM tracking system [3] is to measure the trajectories of charged particles originating from the interactions of heavy-ion beams with nuclear targets. The challenge is to reconstruct the tracks of more than 300 charged particles per central Au+Au interaction with high efficiency and a good momentum resolution. To separate positive and negative particles and to measure their momentum, the central tracking system is located inside the analyzing magnet.

The BM@N hybrid tracking system comprises the 4 silicon stations and 14 GEM stations. The Silicon Tracking System (STS) of the BM@N consists of 4 stations equipped with double-sided micro-strip sensors. The sensors have two sizes 42 mm x 62 mm, and 62 mm x 62 mm, and a thickness of 320. They are located at 30 cm, 50 cm, 70 cm, and 90 cm downstream the target.

The STS is followed by the GEM detectors at 120 cm up to 270 cm, with a gap of 30 cm between the stations. The GEM system consists of 14 GEM detectors (Fig.2): 7 GEM detectors of the size 163×45 cm2 – above the vacuum beam pipe («top GEM detectors»); 7 GEM detectors of the size 163×39 cm2 – below the vacuum beam pipe («bottom GEM detectors»).

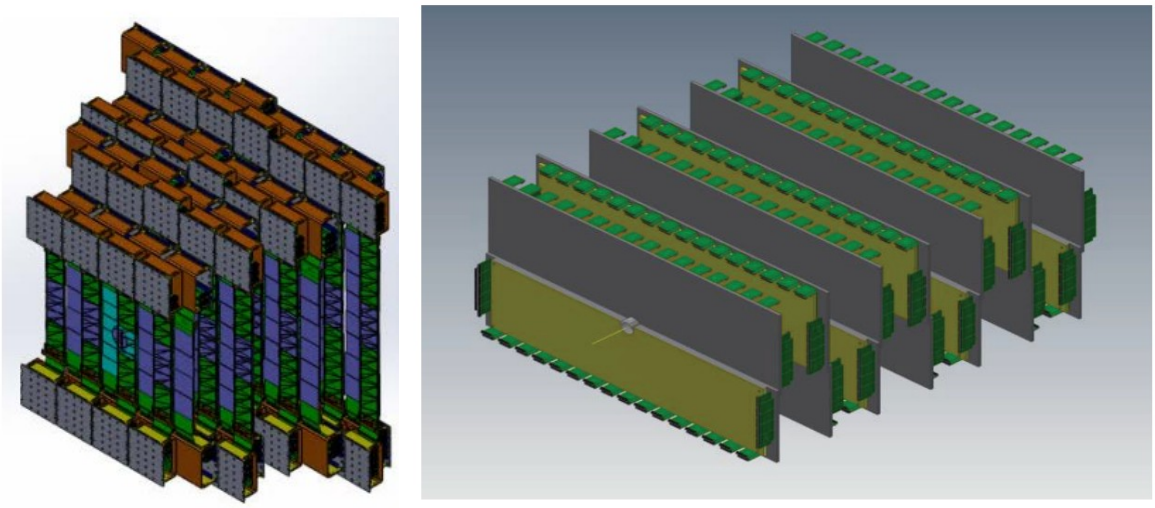

Fig. 2. A technical drawing of the BM@N STS (left) and GEM (right) tracking system.

The momentum of charged particles — products of the interaction of the beam with the target — is measured by the curvature of their trajectories in a magnetic field.

3. TOF-400

The design parameters of the time-of-flight detectors based on a mRPC technology with a strip read-out allows one to perform separation between hadrons (π, K, p) as well as light nuclei with the momentum up to few GeV/c [4].

The high performance time-of-flight (TOF) system together with tracker system based on STS+GEM system must be able to identify charged hadrons and nuclear clusters up to total momentum of 2.5 GeV/c. The fast start detectors (T0) provides the TOF system with the start signal.

The Time-of-Flight system for charged particles identification consists of two walls of Multi-gap Resistive-Plate Chambers. The first wall is positioned at 4 meters from the target (TOF-400), and the second one at the distance of 8 meters (TOF-700). The TOF-400 wall covers about $3\,m^2$ (Fig. 3, Fig.4). The main idea of TOF-400 is identification of charge particles going on big angle with small momentum.

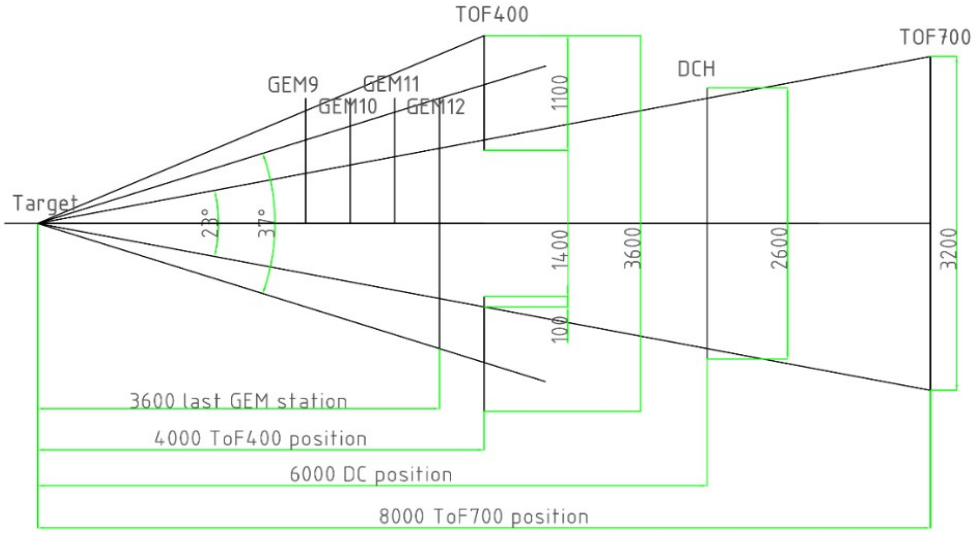

Fig. 3. A scheme of the wall of the TOF-400, TOF-700 detectors in the *zx* plane.

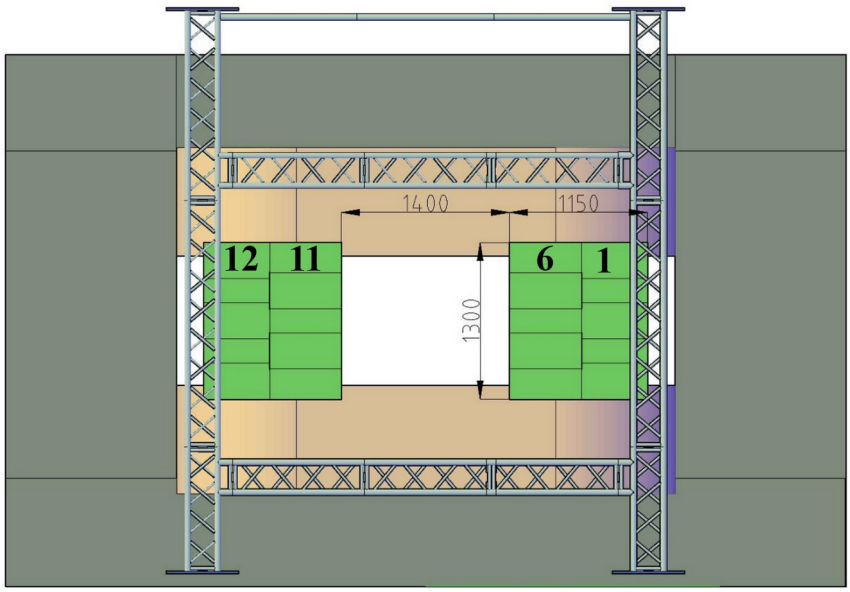

Fig. 4. TOF-400 wall schematic layout. Green squares are active area of mRPCs. Index numbers for the top planes in every module are indicated.

The TOF-400 wall consists of two part (left and right) that are placed symmetrical to the beam. Every part consists of two gas boxes (modules) which each consisting of 5 mRPCs. The active area of the mRPCs overlap on 50 mm inside the box. Gas box made from aluminum frame covered by aluminum honeycomb for reduction of radiation length. Overlap of gas boxes ensures

crossing of active area of detectors 50 mm also. Size of every part is $1.15 \times 1.3\, m^2$ and defined to satisfy the geometrical acceptance of the tracking detectors. Gas boxes mounted on aluminum farm via Bosch profiles for able box position adjustment.

In the work mRPCs are referred to as planes, numbering from 1 to 20. Planes are counted from top to bottom as follow: the first module includes planes 1 to 5, the second module – planes 6 to 10, the third one – planes 11-15, the fourth – planes 16-20 (see fig. 4).

3.1 Mechanical construction of mRPC

A scheme of mRPC is presented on fig. 5 [4]. The detector consists of three stacks of 5 gas gaps each. As resistive electrodes we used common float glass. The outer glass electrodes have thickness 0.42 mm. The internal glass electrodes have thickness 0.27 mm. The fishing line as a spacer defines the 200 μm gap between all resistive electrodes. All internal glasses are floating. The pickup electrodes look like strips and made on the PCB board. The main feature of the proposed triple-stack mRPC is that readout strips are located only in the inner stack. This ensures that the construction is symmetric, and speed of signals on the anode and cathode are the same, what prevent the dispersion of the signal.

Differential analog signal from strip is transferred by twisted pair cable to front-end electronics. Signal is reading out from both ends of the strip. It provides better time resolution and determination of the coordinate of a particle along strip. For stiffening structure we glue paper honeycomb with a thickness of 10 mm on outer part of the external PCBs. Dimension of active area of one mRPC is $300 \times 600\, mm^2$. It has 48 readout strips, 10 mm wide and 300 mm long. To reduce crosstalk the gap between strips is 2.5 mm.

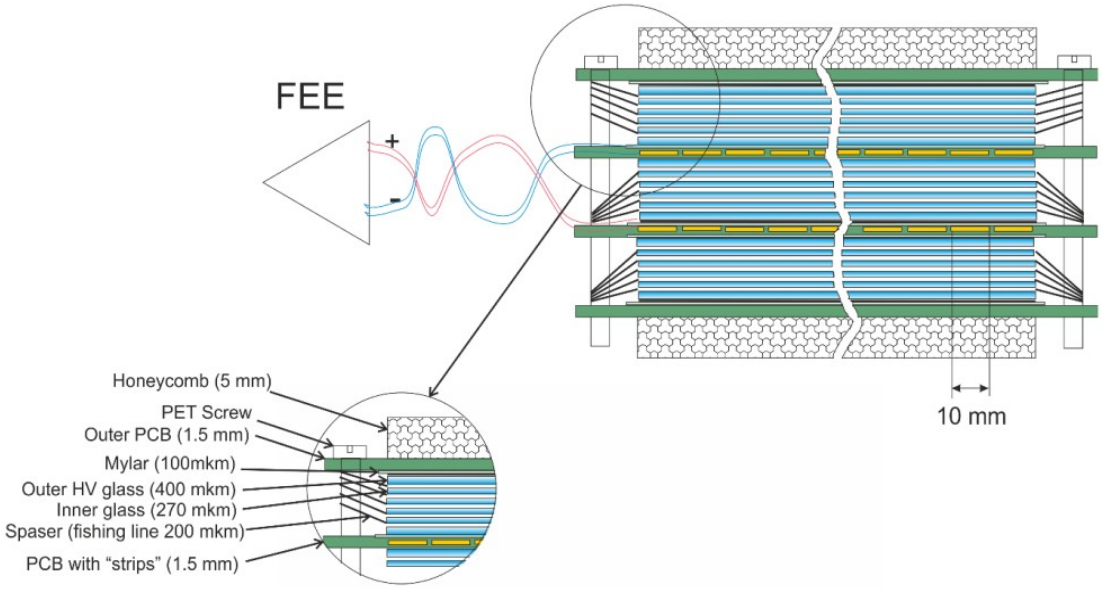

Fig. 5. Sectional view of the triple stack strip mRPC for TOF-400.

Alignment of TOF-400 detector

1. Problem statement

The particles produced in the collision go through the STS+GEM tracking system placed in a magnetic field and then hit the TOF-400 detector. A passing particle leaves a signal in one of the planes, and in this place the hit of the particle will be reconstructed by the reconstruction algorithms. The accuracy of hit reconstruction is determined by two main factors. The first is the internal resolution of the detector, and the second is the measurement of the position of the detector in the global reference frame. In the first approximation, the position of the planes is known from the results of measurements of the module surfaces position after the assembly of the detector, but it is not possible to determine the planes position more precisely when they are sealed inside the modules. The purpose of the alignment procedure is to reduce the error due to the uncertainty of the planes position. This is achieved by calculating position corrections for each plane in the system. The calculated corrections are added to the geometry description used by the reconstruction algorithms.

2. The correction calculation method.

In our work we use method, which allows determination of the corrections along Z axis – dz – via analysis of $dy\,vs\,Ty$ and $dx\,vs\,Tx$ distribution, where dy, dx – residuals along y, x axes respectively, Ty, Ty – entry angle tangents of tracks, propagated to the TOF-400, along y, x axes respectively (fig. 6).

Tracks reconstructed in the STS+GEM tracking system are extrapolated to TOF-400. The intersection point of the extrapolated track with the plane is characterized by the x coordinate of the hit and the of entry angle α of the track, at which it intersects the plane of the TOF-400 detector. At the initial stage, this geometry does not contain corrections. Along with this point, the hit with the coordinates z_{real}, x_{hit} is reconstructed. If we consider a triangle in the xOz plane (Fig. 6) with the cathet dx and the adjacent angle α, where dx is the difference between the intersection coordinate of the track with the plane and the hit coordinate, and α is the specified angle of entry, then it can be obtained that the discrepancy dx is associated with the displacement dz along z axis through the tangent of the entry angle. Considering a similar triangle in the yOz plane, one gets the same relation for the dy and Ty. Thus, either of the two dependencies gives the desired corrections to the position of the dz planes.

Since this reasoning works the for both planes – xOz and yOz – the same way, similar correction values are expected when considering both types of distributions. It is also reasonable to expect close correction values for the planes in the same module, i.e. the planes 1-5, 6-10, 11-15, 16-20.

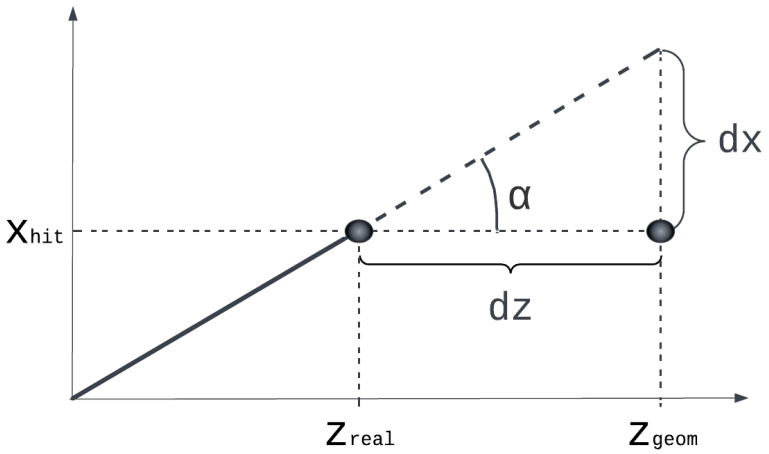

Fig. 6. To the description of the method for correction calculation.

3. Data for alignment procedure

To perform the alignment procedure the data from a physics run session carried out in December 2022 — February 2023 were used. The beam is Xe, the target is CsI. Physical runs with a magnetic field were used, those are Runs 7829+7830 (collision energy 3.8 AGeV, 2 million events)as well as the calibration run with a magnetic field turned off, which is Run 8307 (collision energy 3.8 AGeV, 311 thousand events).

4. Alignment procedure

To perform the alignment procedure, The BmnRoot framework was being used for calculations. In the calculations, tracks from the STS+GEM tracking system are extrapolated to TOF-400. In the calculation process there were a few options, regarding whether we should specify the sort of particles for track propagation or not. The reasons in that outside the magnet there is magnetic residual, which may affect the propagation result in case of different sorts of particles used for performing the propagation. Thus the first task was to determine whether there are differences in the results of calculations when using particles of different sort for propagation. To do so, three calculations were carried out: propagation in the assumption that all particles are protons only; propagation with positively and negatively charged pions (distinguished by the particle momentum sign); propagation by protons and antiprotons. No discrepancies were found in the results, so it was decided to carry out all calculations setting propagation of tracks with protons only.

Next step was to prepare a new macro file for BmnRoot so the preidentification of particles could be made. Essentially, we built distributions of the type β *vs* p (fig. 7, top picture), where β is the particle velocity parameter and p is particle momentum. Such a distribution was created for each plane in run with magnetic field on, and the analytical expression for $\beta(p,m)$ dependence was used to plot it on the each distribution. Here m is the mass of a particle (proton or pion), acts as a parameter.

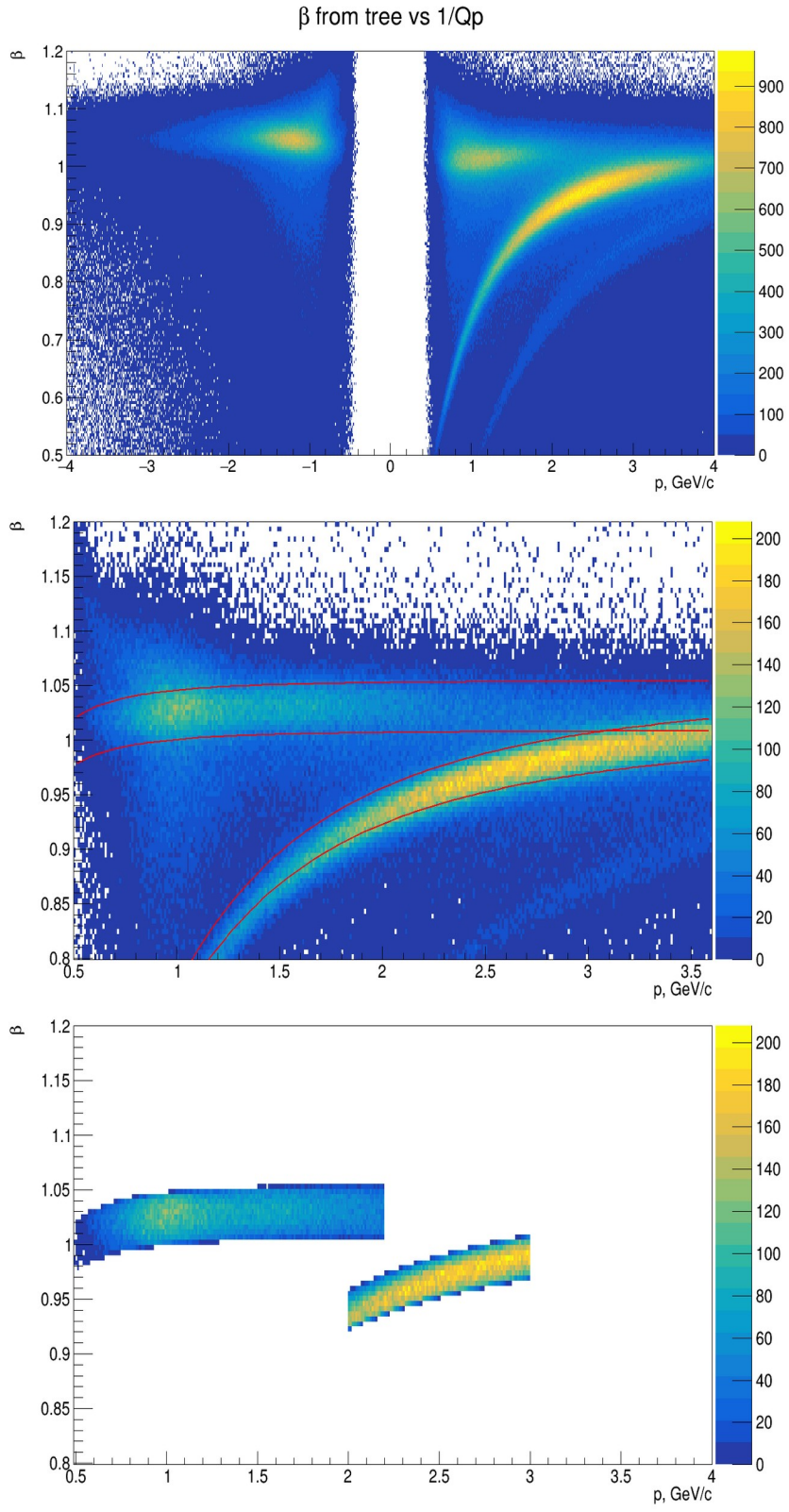

Fig. 7. Particle preidentification performed using $\beta(p,m)$ analytical dependence..

Having plotted those dependencies on our distributions, we are able to see clearly which light stripes correspond to protons, positively charged pions and negatively charged ones, as it is shown on the fig. 7, bottom pictures. One can also see from looking at the pictures that we cut out particle of specific momentum range. For pions this range was (0; 2.2) GeV/c – ones with higher momenta are unlikely to be pions actually. For protons the range was set to (2; 3) GeV/c. The

reason of that is illustrated in Figure 8. On the distribution of residuals along x axis against the momentum values of particles dx *vs* p, one can see a "tail" in the area of small momenta: protons with small values correspond to large discrepancies between the hit coordinate in the plain and the coordinate of the track propagated to the plain. It is suggested that the reason may be an underestimation of the momentum: the curvature radius of the particle tracks with small momenta is greater than that of ones with higher momenta, therefore the deviation of the track coordinate in the plane from the hit coordinate is greater as well. So the cut on the momentum value was made to exclude the possible influence of this effect on further results.

We should notice that for pion such a tail is present as well. However, we have not set cut on pions momenta since for further alignment procedure we used distributions for protons only.

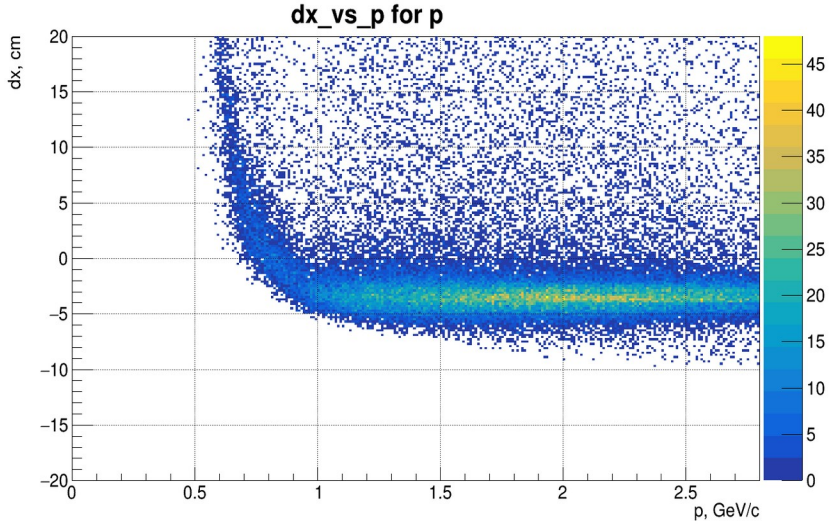

Fig. 8. dx *vs* P distribution for protons, experimental data.

After the predentification had been performed, we built the residuals distributions, dy *vs* dx, for every plane and, for each given plane, every sort of particles hitting the plane. For Runs 7829+7830 with the magnetic field on, we noted the difference in the in the residual distributions dy *vs* dx for protons and negatively charged pions (Fig. 9). For instance, for the 10th plane, the average values of residuals for protons along x and y axes are respectively (0.511; 0.694), while for negatively charged pions those are (2.140; 1.840). Thus, the particle sign dependence of the distribution took place. We assumed that this difference is a consequence of the misalignment along z axis.

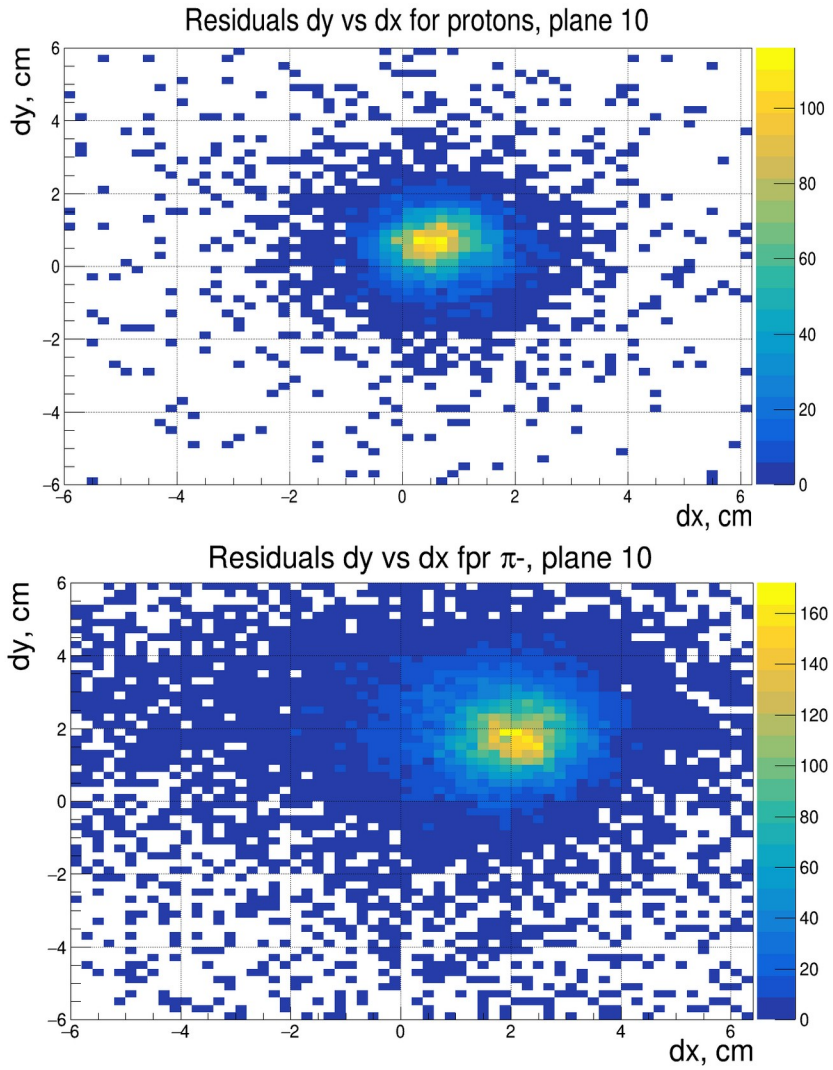

Fig. 9. *dy vs dx*distribution for protons and negatively charged pions with the example of the 10th plane for experimental data.

To test the hypothesis, we ran the Monte Carlo simulation and built similar distributions. It should be noted that a shift at -6 cm along *z* axis was introduced into the MC simulation in order to satisfy the geometry used to perform alignment procedure according to experimental data.

Figure 10 shows that even when the same position of TOF-400 along *z* axis is set, the negatively charged pions and protons are shifted relative to each other. Here one can see the shift of residual spot along *x* axis, with the average residual for protons being $-0.2\,cm$, and for negatively charged pions being $-1.9\,cm$.

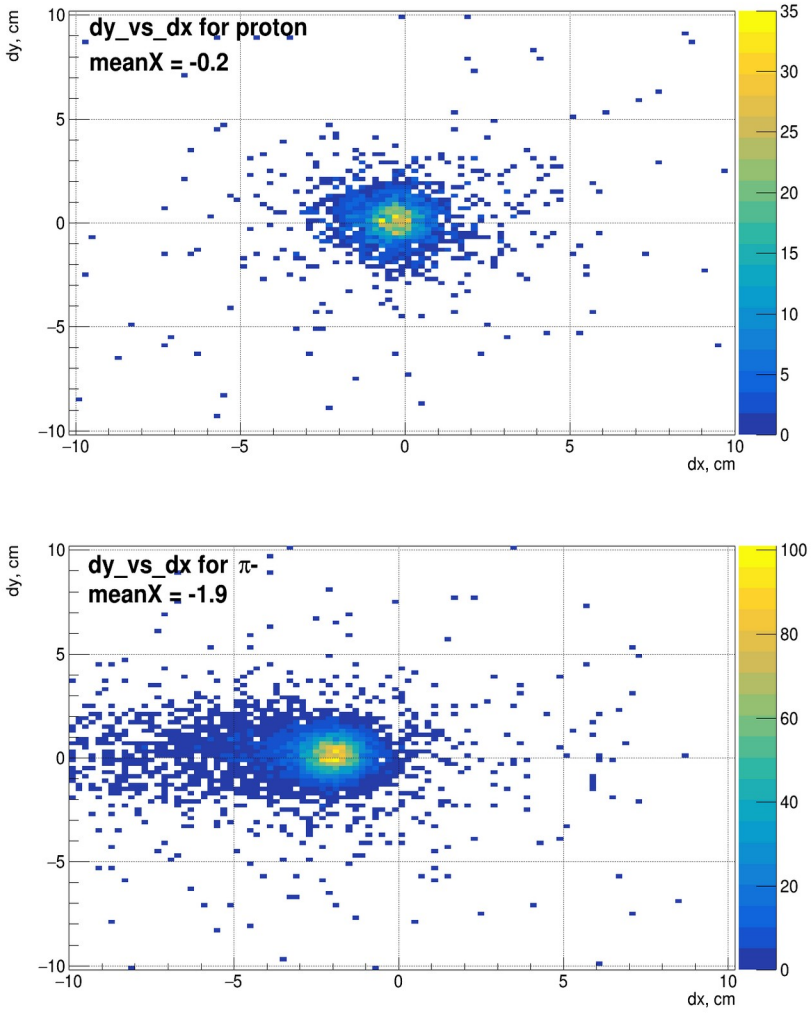

Fig. 10. The distribution of *dy vs dx* for protons and negatively charged pions with the example of the 10th plane for MC modeling.

We are also pointing out that there is a "tail" on the *dx vs p* distribution (Fig. 11), similar to the distribution according to experimental data, for both calculations with a shift of $dz = -6\,cm$ (top) and without it (bottom). Since the tail is obtained for both simulation and experimental data, and with and without the shift, it may not be the consequence of the misalignment.

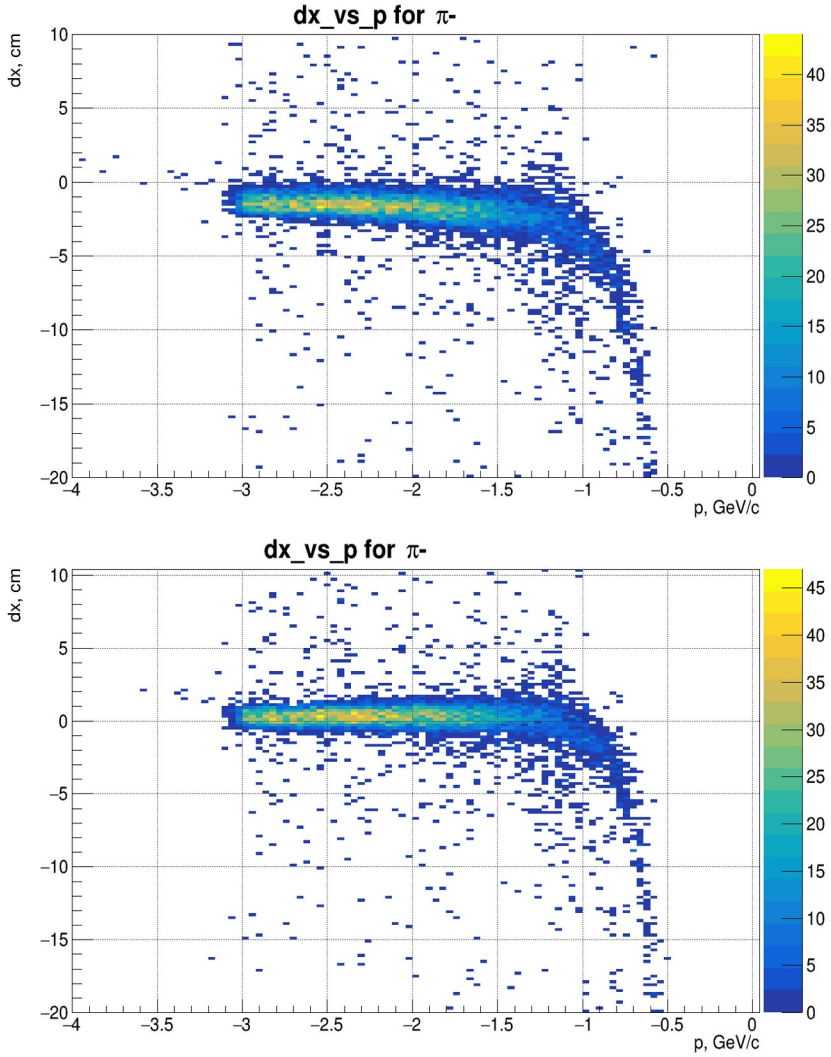

Fig. 11. $dx\,vs\,P$ distribution for negatively charged pions, MC data. The shift $dz=-6\,cm$ is introduced in the caculation on the top picture, and there is no shift on the bottom one.

At the next step it was necessary to obtain those values of the tangents of the angles of occurrences Tx (Ty) for each plane which are of our interest because they are the desired corrections for z placement of planes. Here we consider Runs 7829+7830 with magnetic field on.

This was made as follows (Fig. 12): in the distribution of $dx\,vs\,Tx$, projections of bins along the x axis (Tx) axis were taken to the y axis (dx) for each plain. Each projection was fitted by a Gaussian curve, and the mean and standard deviation of this fit, together with the x-coordinate of the bean in cm, were added to the graph created for this specific distribution: the mean is the y coordinate of the point in the graph, the deviation is an error. The graph was superimposed on the $dx\,vs\,Tx$ distribution. Then a set of points corresponding to the bins with the largest number of entries was selected, and this points of the graph were fitted with a straight line. The parameter $p1$ of this fit gives the value of the dz correction for this plane. The same was done for the $dy\,vs\,Ty$ distributions for each plane.

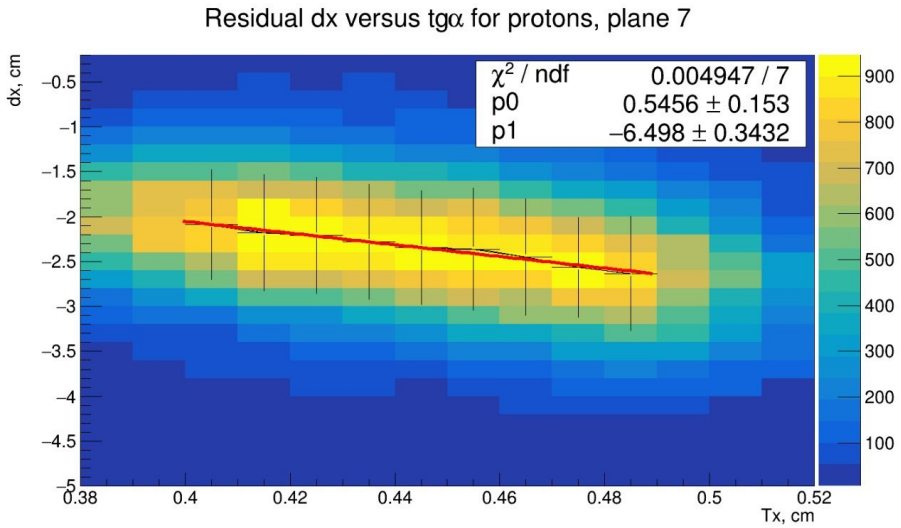

Fig. 12. Illustrations of the algorithm for obtaining *dz* corrections as a result of the graph fitting according to the distribution *dx vs Tx*.

After the fitting procedure, two graphs of corrections *dz* versus plane number were built. They are shown in Figure 13 (the numbering of the planes on these graphs starts from zero, i.e. 0 – 19).

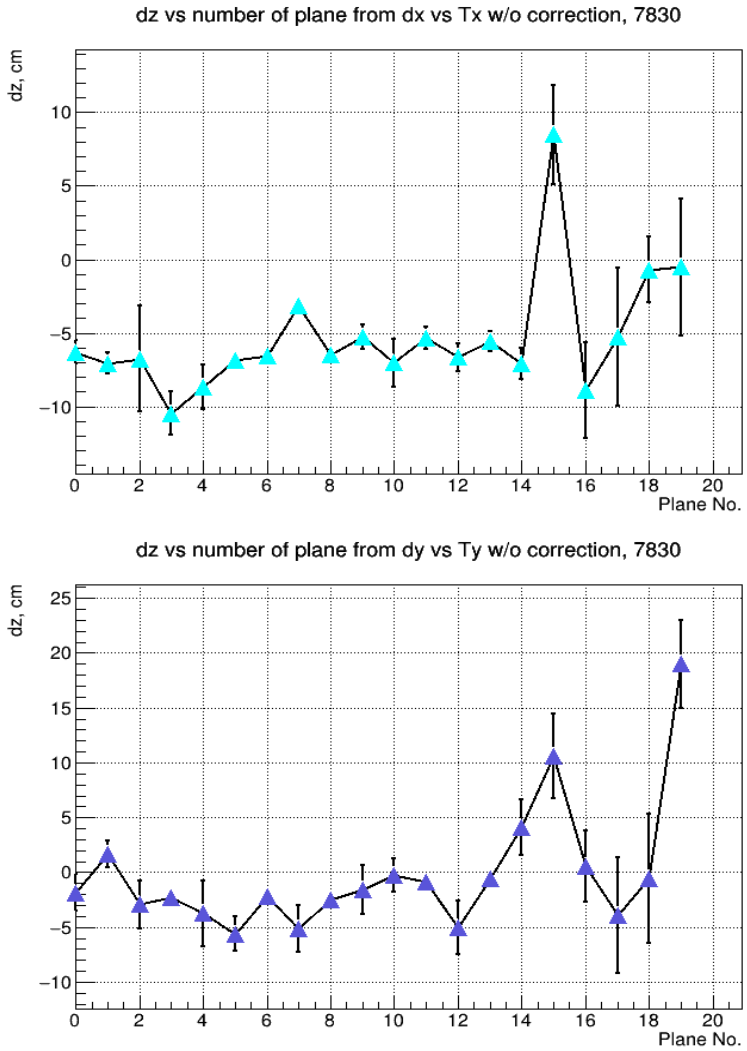

Fig. 13. Distribution of the received corrections for each plain according to the distribution *dx vs Tx* (top) and *dy vs Ty* (bottom), Runs 7829+7830 (with magnetic field turned on).

The variation of values was found out to be too large to consider the result satisfactory. Firstly, within one module, the magnitude of the corrections may exceed the thickness of the module itself or imply such a displacement of planes that would lead to the intersection of neighboring planes. Secondly, there is no good match between the results obtained using *dx vs Tx* and *dy vs Ty* distributions for the planes of one number.

At this point, we decided to turn to Run 8307 — with magnetic field turned off, so the tracks are straight lines, and deviations are a consequence of the particle interaction with matter only. The following displacement values were obtained for this Run (Fig. 14). Again, one can see a large deviation of *dz* values.

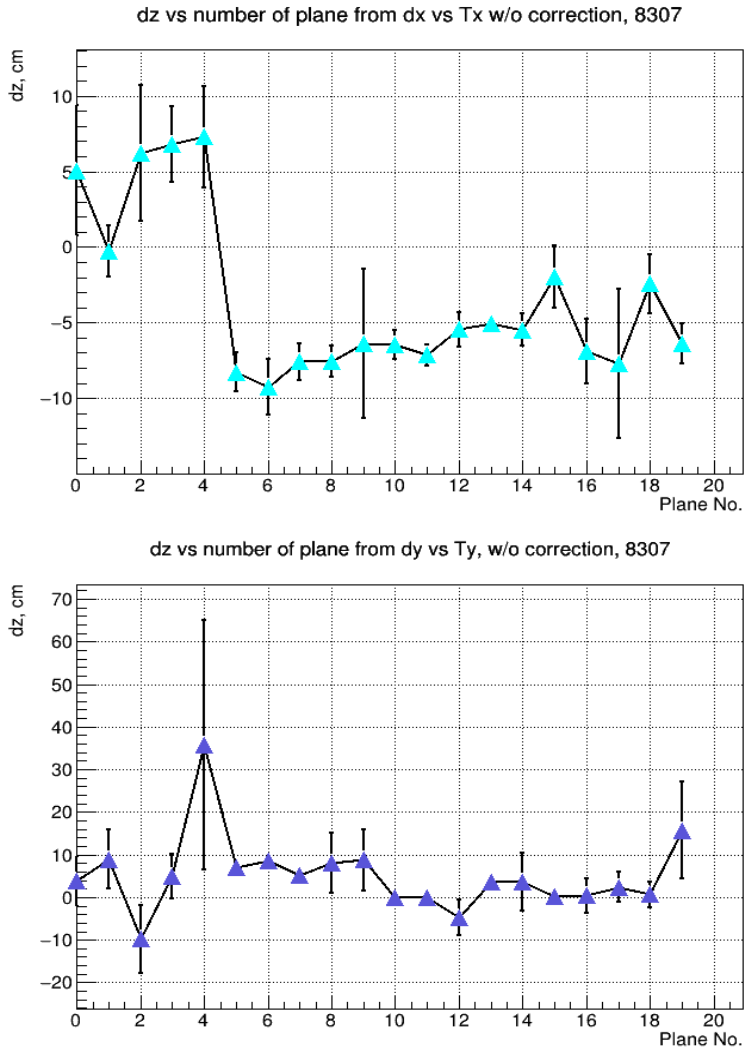

Fig. 14. Distribution of the *dz* corrections for each plain according to the distribution *dx vs Tx* (top) and *dy vs Ty* (bottom), Run 8307 (no magnetic field).

After thorough check of our scripts for calculations, an error was found in the geometry used to propagate tracks to the TOF-400. This error might affect the accuracy of results. In this regard, a displacement of all planes in z-direction was made, the value of this displacement was $dz = +6.5\,cm$. Having the fitting procedure performed once again, the following results for Runs 7829+7830 and 8307 were obtained (Fig. 15).

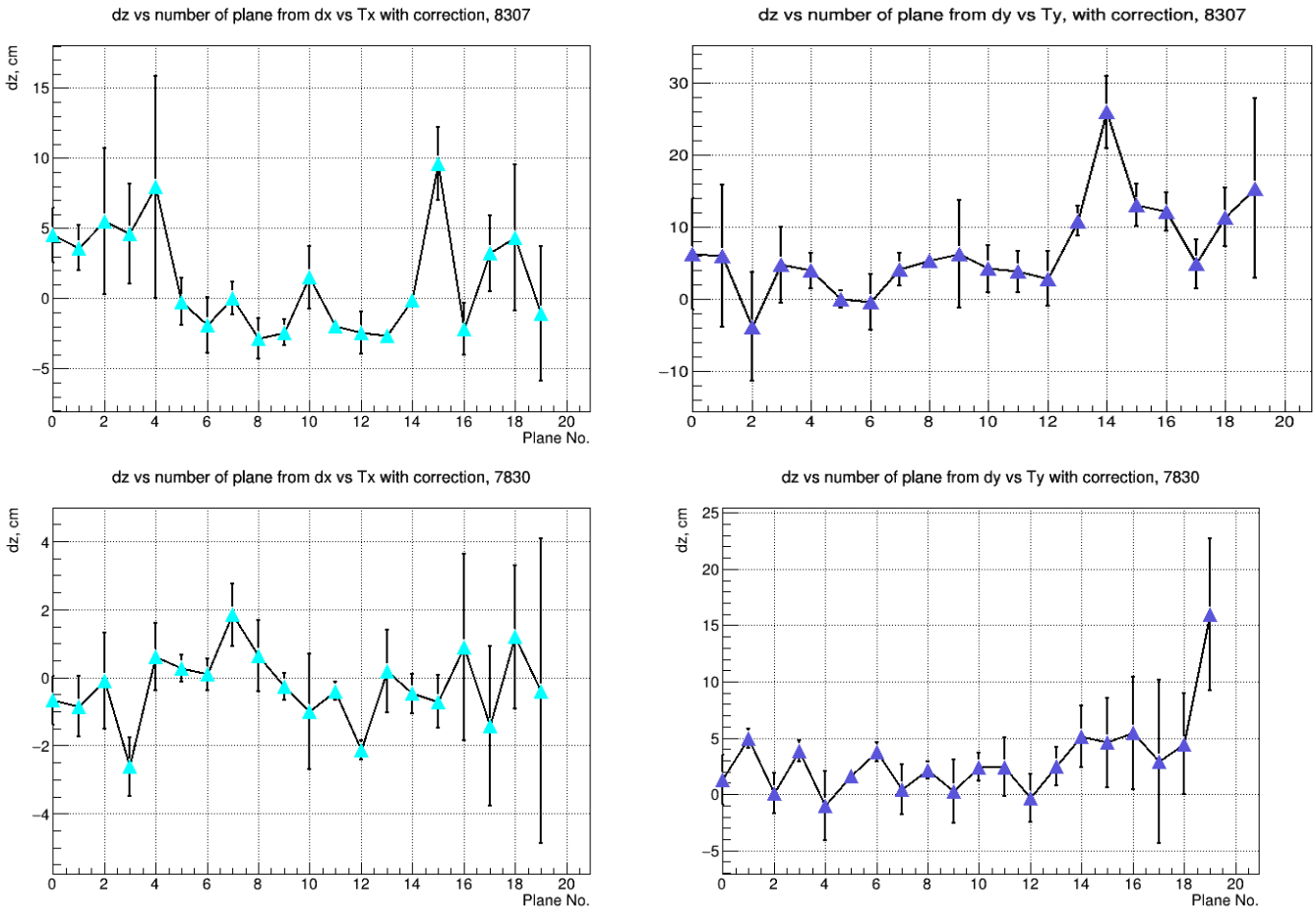

Fig. 15. Distribution of the obtained corrections for each plain according to the distribution *dx vs Tx* (left) and *dy vs Ty* (right), Run 8307 (no magnetic field) - at the top, Runs 7829+7830 (with magnetic field on) - at the bottom.

For the Calibration Run 8307 with no magnetic field, the distribution obtaines using *dx vs Tx* became smoother, but one using *dy vs Ty* was still significantly uneven. The reason may be low statistics, which complicates the fitting of both bins with Gaussians and graphs with straight lines.

For Runs 7829+7830, the shift of planes improved the result at least for *dx vs Tx*, where the values became closer to 0. However, if one compares *dx vs Tx* and *dy vs Ty* for one specific Run, then the distribution over *dx vs Tx* has fewer severe fluctuations. Regarding to the last planes, 19 and 20 (18 and 19 in these pictures), they are located pretty far from tbe beam pipe, thus often show bad result for fitting due to low statistic (see fig.15, two bottom pictures). Notice, that pictures have different scale of vertical axes.

After a correction for the error had been introduces, the distributions of residuals *dy vs dx* were built again (Fig. 16) for protons and negatively charged pions to check if there still was a discrepancy for particle of opposite signs. Here we got the average for protons $¿dy>¿1.9\,cm$, $¿dx\geq-0.1\,cm$; for pions it was $¿dy>¿0.9\,cm$,$<dx\geq0.08\,cm$. Using the example of one plane, it is shown that the distribution is almost aligned along *x* axis (residuals *dx*), while the difference in *dy* between protons and negatively charged pions is 1 cm.

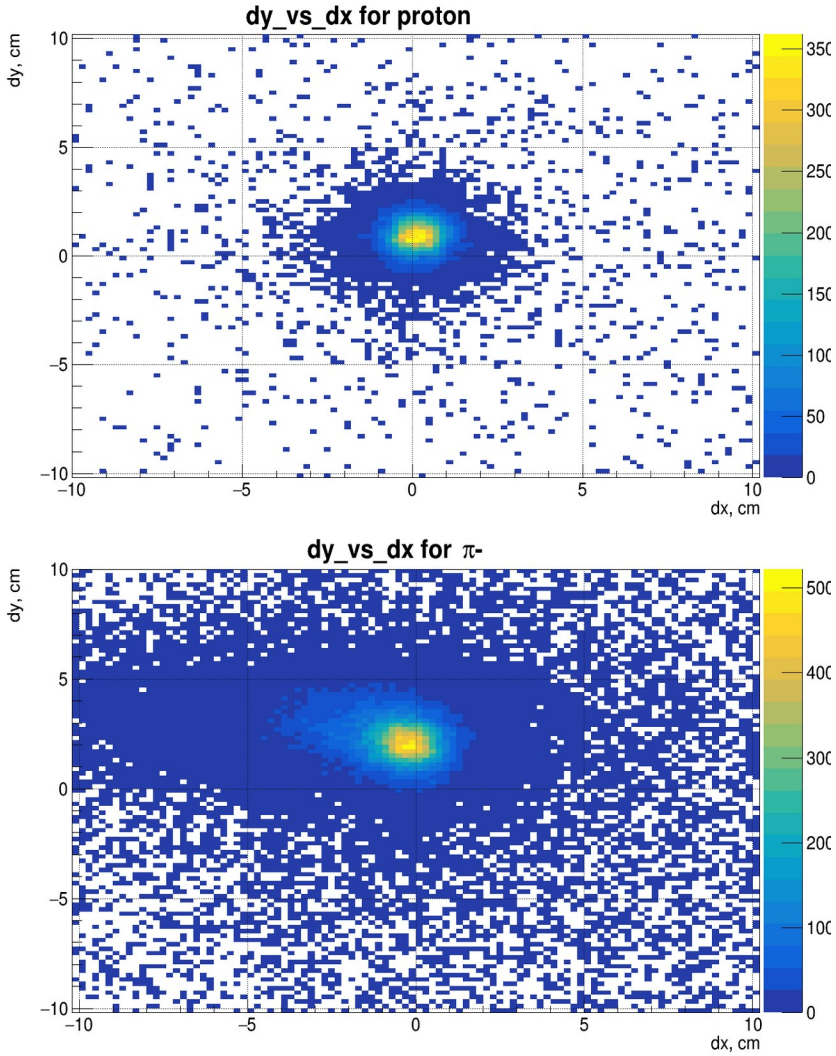

Fig. 16. *dy vs dx* distribution for protons (top) and negatively charged pions (bottom) after the correction for the error in geometry.

Besides the graphs for the *dz* vs Plane Number, representing the result of the work visually, in the Appendix the exact values of displacement are provided for each plane in two runs, 7829+7830 and 8307, obtained with $dx\,vs\,Tx \wedge dy\,vs\,Ty$.

Conclusion

The method of determining the TOF-400 misalignment by correlation $dx\,vs\,Tx\,(dy\,vs\,Ty)$ gives a significantly big variation of values for correction along *z*-axis, that is not negligible. If the TOF-400 was shifted according to the obtained values, then one would get the intersection of planes in the geometry. At the moment, the method used in the work does not seem to be appropriate for carrying out the TOF-400 detector alignment procedure.

In the process of work, an error was found in the description of the TOF-400 geometry. An attempt was made to check the alignment of the system with the corrected geometry. The values of the displacements have become more reasonable, although they still cannot be called satisfactory.

The further work is needed to find out whether this method can be adjusted to get more accurate corrections or new one have to be implemented for TOF-400 alignment in the latest physics run session at BM@N experiment.

References

1. D. Baranov et al 2017 JINST 12 C06041
2. Guber, F. & Borisenko, Daria & Finogeev, D. & Golubeva, M. & Ivashkin, A. & Karpushkin, Nikolay & Morozov, Sandra & Senger, A.. (2019). New forward hadron calorimeter for centrality and reaction plane determination at BM@N heavy ion experiments. EPJ Web of Conferences. 204. 07007. 10.1051/epjconf/201920407007.
3. Technical Design Report of the Silicon Tracking System as Part of the Hybrid Tracker of the BM@N Experiment.
4. Technical Design Report of the Time of Flight System (TOF-400) BM@N.

Appendix A

Run 7829+7830 with magnetic field								
Plane No	Results before the shift $dz = 6.5\,cm$ to correct for the error				Results after the shift $dz = 6.5$ to correct for the error			
	corrections by dx vs Tx		corrections by dy vs Ty		corrections by dx vs Tx		corrections by dy vs Ty	
	Correc-tion	Error	Correc-tion	Error	Correc-tion	Error	Correc-tion	Error
1	-6.288	0.827	-1.839	1.651	-0,671	0.724	1.26	2.224
2	-7.046	0.699	1.693	1.229	-0.844	0.878	4.962	0.886
3	-6.752	3.584	-2.9	2.182	-0.088	1.405	0.104	1.757
4	-10.48	1.472	-2.313	0.655	-2.617	0.854	3.85	0.933
5	-8.659	1.513	-3.733	2.997	0.624	0.99	-1.031	3.063
6	-6.832	0.232	-5.614	1.561	0.270	0.403	1.673	0.656
7	-6.547	0.44	-2.143	0.279	0.091	0.456	3.78	0.855
8	-3.146	0.261	-5.15	2.131	1.845	0.927	0.418	2.204
9	-6.446	0.324	-2.471	0.39	0.628	1.047	2.149	0.793
10	-5.279	0.819	-1.581	2.218	-0.269	0.388	0.241	2.818
11	-7.039	1.629	-0.247	1.483	-1.01	1.697	2.44	1.266
12	-5.348	0.75	-0.895	0.594	-0.394	0.258	2.434	2.59
13	-6.663	0.982	-5.001	2.424	-2.119	0.287	-0.355	2.123
14	-5.58	0.69	-0.539	0.697	0.189	1.217	2.514	1.697
15	-7.115	1.062	4.125	2.534	-0.475	0.581	5.129	2.698
16	8.485	3.38	10.58	3.862	-0.708	0.783	4.589	3.945
17	-8.894	3.273	0.553	3.242	0.891	2.735	5.444	5.003
18	-5.286	4.686	-3.897	5.307	-1.429	2.352	2.911	7.263
19	-0.695	2.237	-0.573	5.914	1.192	2.113	4.495	4.455
20	-0.504	4.646	19	4.004	-0.391	4.483	16.0	6.733

Run 8307 with no magnetic field								
Plane No	Results before the shift $z=6.5$to correct for the error				Results after the shift $z=6.5$to correct for the error			
	corrections by *dx vs Tx*		corrections by *dy vs Ty*		corrections by *dx vs Tx*		corrections by *dy vs Ty*	
	Correc-tion	Error	Correc-tion	Error	Correc-tion	Error	Correc-tion	Error
1	5.065	4.319	3.79	5.82	4.545	1.949	6.304	7.735
2	-0.279	1.714	8.941	6.926	3.606	1.617	6.064	9.845
3	6.243	4.482	-9.795	8.038	5.495	5.208	-3.777	7.527
4	6.803	2.484	4.927	5.252	4.651	3.564	4.821	5.283
5	7.291	3.346	35.78	29.29	7.953	7.913	4.005	2.454
6	-8.264	1.262	6.928	1.796	-0.224	1.695	0.0262	1.186
7	-9.246	1.871	8.483	0.786	-1.900	1.967	-0.322	3.893
8	-7.59	1.225	5.31	0.423	0.003	1.186	4.209	2.265
9	-7.576	1.013	8.008	7.062	-2.859	1.45	5.351	0.512
10	-6.388	4.96	8.745	7.204	-2.411	0.941	6.331	7.521
11	-6.452	0.9304	0.086	1.916	1.516	2.212	4.283	3.283
12	-7.143	0.7094	0.056	1.201	-1.953	0.534	3.862	2.911
13	-5.456	1.169	-4.626	4.194	-2.420	1.527	2.904	3.82
14	-5.065	0.488	3.554	1.513	-2.654	0.346	10.9	2.032
15	-5.482	1.056	3.682	6.823	-0.127	0.191	25.99	5.018
16	-1.956	2.043	0.174	0.147	9.633	2.619	13.15	2.918
17	-6.914	2.148	0.473	4.07	-2.192	1.848	12.14	2.675
18	-7.724	4.931	2.447	3.462	3.225	2.717	4.938	3.434
19	-2.432	1.969	0.714	2.988	4.36	5.19	11.4	4.062
20	-6.398	1.329	15.75	11.39	-1.073	4.797	15.42	12.49